AGU PUBLICATIONS

Geochemistry, Geophysics, Geosystems

RESEARCH ARTICLE
10.1002/2015GC005784

Special Section:
The Lithosphere-Asthenosphere System

The thinning of subcontinental lithosphere: The roles of plume impact and metasomatic weakening

Hongliang Wang[1], Jeroen van Hunen[1], and D. Graham Pearson[2]

[1]Department of Earth Sciences, Durham University, Durham, UK, [2]Department of Earth and Atmospheric Sciences, University of Alberta, Edmonton, Alberta, Canada

Key Points:
- The hypothesis that mantle plume remove continental lithosphere is tested
- The effect of mechanical erosion by plumes on cratonic root is very limited
- Metasomatism weakening is essential to remove originally stable lithosphere

Correspondence to:
H. Wang,
hongliang.wang@dur.ac.uk

Citation:
Wang, H., J. Hunen, and D. Graham Pearson (2015), The thinning of subcontinental lithosphere: The roles of plume impact and metasomatic weakening, *Geochem. Geophys. Geosyst.*, *16*, 1156–1171, doi:10.1002/2015GC005784.

Received 17 FEB 2015
Accepted 13 MAR 2015
Accepted article online 27 MAR 2015
Published online 28 APR 2015

Abstract Geologically rapid (tens of Myr) partial removal of thick continental lithosphere is evident beneath Precambrian terranes, such as North China Craton, southern Africa, and the North Atlantic Craton, and has been linked with thermomechanical erosion by mantle plumes. We performed numerical experiments with realistic viscosities to test this hypothesis and constrain the most important parameters that influence cratonic lithosphere erosion. Our models indicate that the thermomechanical erosion by a plume impact on typical Archean lithospheric mantle is unlikely to be more effective than long-term erosion from normal plate-mantle interaction. Therefore, unmodified cratonic roots that have been stable for billions of years will not be significantly disrupted by the erosion of a plume event. However, the buoyancy and strength of highly depleted continental roots can be modified by fluid-melt metasomatism, and our models show that this is essential for the thinning of originally stable continental roots. The long-term but punctuated history of metasomatic enrichment beneath ancient continents makes this mode of weakening very likely. The effect of the plume impact is to speed up the erosion significantly and help the removal of the lithospheric root to occur within tens of Myr if affected by metasomatic weakening.

1. Introduction

The contrasting composition and heterogeneity between ancient cratonic and oceanic lithosphere is one of the most salient features of modern plate tectonics. Thick Archean cratonic lithosphere is generally considered to be stable and dynamically inactive since it was formed. However, the discovery that the North China Craton (NCC) has lost a significant part of its root in the Mesozoic [*Gao et al*., 2002; *Zhu and Zheng*, 2009] shows that cratons are not isolated features in Earth's dynamic system. The chemical distinction of highly melt-depleted cratonic roots is considered to be the most important reason for the survival of Archean lithosphere [*Boyd*, 1989; *Carlson et al*., 2005]. Geodynamical research supports this hypothesis through numerical modeling by using reasonable density structure and mantle rheology [*Doin et al*., 1997; *Lenardic and Moresi*, 1999; *O'Neill et al*., 2008; *Wang et al*., 2014].

Increasing evidence due to the development of modern geochemical and petrological techniques shows that many Precambrian terranes have experienced some degree of progressive, multistage modification (or enrichment) to their roots through mantle metasomatism [e.g., *Carlson et al*., 2005; *Hanghøj and Kelemen*, 2001; *Simon et al*., 2003; *Chesley et al*., 2004; *Sand et al*., 2009; *Janney et al*., 2010; *Tappe et al*., 2011; *Tang et al*., 2013; *Smit et al*., 2014], even though such roots appear to be mostly physically stable. Seismic tomography further indicates the widespread refertilization of Archean lithosphere by mantle thermal events, e.g., the Bushveld and Karoo events in the Kalahari craton [*James et al*., 2001; *Griffin et al*., 2003a]. Through fluid/melt-rock interaction, metasomatic refertilization might increase the density and weaken the rheology of subcontinental lithospheric mantle (SCLM) and thus affect its stability [*Schutt and Lesher*, 2010]. By decreasing the Mg number (Mg#) of the originally depleted continental lithosphere and raising its pyroxene and garnet content, the enrichment of the depleted mantle could reduce the chemical buoyancy of SCLM significantly [*Pearson and Nowell*, 2002; *Griffin et al*., 2003b; *Carlson et al*., 2005; *Pearson and Wittig*, 2008; *Gibson et al*., 2013]. Metasomatic processes might also have a weakening effect on the rheology of the constituent peridotites by adding water to the originally dry, depleted continental root [*Peslier et al*., 2012]. Moreover, research on the Slave craton in Canada indicates that metasomatism may affect the mantle rheology based on the correlation between elastic thickness and mantle composition [*Poudjom Djomani et al*., 2005]. Hence, the accumulating evidence that metasomatic refertilization affects both the compositional buoyancy and

the rheology of the SCLM and leads to the possible destabilization of thick lithospheric roots, provides the motivation to numerically simulate this process to constrain the overall controls.

Although most Precambrian terranes appear to have been geologically stable/inactive, many have experienced some degree of thinning or recycling [*Lee et al*., 2011], such as the North China Craton (NCC) [*Gao et al*., 2002], the Wyoming craton [*Carlson et al*., 2004], the Colorado plateau [*Levander et al*., 2011], the Proterozoic lithosphere around the Kaapvaal craton [*Bell et al*., 2003; *Mather et al*., 2011], and the North Atlantic Craton (NAC) [*Tappe et al*., 2007]. The destruction of the NCC appears to be a unique example of complete removal of the cratonic root and has received a lot of attention recently [*Zhu and Zheng*, 2009]. With its abundant kimberlite pipes, the Kaapvaal craton of southern Africa provides a good natural laboratory to study the modification and evolution of Precambrian lithosphere [*Simon et al*., 2003; *Griffin et al*., 2003a; *Gibson et al*., 2008; *Kobussen et al*., 2008]. *Carlson et al*. [2005] suggested that the loss of buoyancy through mantle metasomatism is a possible mechanism that could rapidly transfer the continental lithospheric mantle into the asthenosphere and cause intracontinental deformation and volcanism. These events might, in some cases, lead to continental breakup [*Tappe et al*., 2007]. The increased temperatures and flow stress related to mantle plume impact provide another, perhaps related mechanism for the lithosphere removal events [*Ebinger and Sleep*, 1998; *Sleep et al*., 2002; *Bell et al*., 2003].

Geodynamical modeling has long been used to study the general mantle dynamics of plume-lithosphere interaction [*Ribe and Christensen*, 1994; *Nyblade and Sleep*, 2003; *Van Hunen and Zhong*, 2003; *François et al*., 2012], but the mechanical erosion and thinning of the continental lithosphere has received less attention. *Sleep et al*. [2002] demonstrated that a cratonic root can deflect plume material and convection can focus on the edge of the root, which could lead to a reduction of the root width. *Morency et al*. [2002] found that, depending on the width of the cratonic block, it takes 50–750 Myr to convectively remove a 250 km thick cratonic root if the lithosphere has an equilibrium thickness of about 100 km, but the chemical heterogeneity of continental lithosphere and plume events was not considered in their study. *Guillou-Frottier et al*. [2012] argued for several different plume-induced dynamical instabilities near the cratonic root to explain the P-T-t paths recorded by the metallogenic data from South Africa. These studies do not explicitly explore the role of compositional buoyancy and strengthening on cratonic mantle dynamics for a situation in which a plume impacts on the subcontinental root. In particular, metasomatic refertilization could change the chemical heterogeneity of mantle lithosphere and may have important geodynamical consequences.

In this study, we perform new numerical experiments to explore how the buoyancy and rheology of subcontinental lithosphere affect plume-continent interaction and study the mechanism of lithosphere removal. The potential mechanisms of lithosphere removal underneath Precambrian terranes such as southern Africa and the NCC will be discussed based on the numerical results.

2. Model Description

2.1. Governing Equations

We use a Cartesian version of the finite element code Citcom [*Moresi and Solomatov*, 1995; *Zhong et al*., 2000; *Van Hunen et al*., 2005] to solve the incompressible flow with the extended Boussinesq approximations [*Christensen and Yuen*, 1985; *King et al*., 2010]. It solves the following nondimensional governing equations for mass, momentum, and energy conservation:

$$\nabla \cdot \mathbf{u} = 0 \tag{1}$$

$$-\nabla P + \nabla \cdot \left(\eta\left(\nabla \mathbf{u} + \nabla \mathbf{u}^T\right)\right) + (RaT - Rb_i C_i)e_z = 0 \tag{2}$$

$$\frac{\partial T}{\partial t} + (u \cdot \nabla)T = \nabla^2 T + Q_0 + \frac{Di}{Ra}\eta\dot{\varepsilon}^2 + Di(T + T_s)u_z \tag{3}$$

In these equations, a standard nondimensionalization is used, with $x = x'h, t = t'h^2/\kappa, \eta = \eta'\eta_0$, where in the equations above, the primes of the nondimensional parameters are dropped for clarity. The dimensional physical parameters are listed and explained in Table 1. The thermal and chemical Rayleigh number Ra and Rb_i are defined as

Table 1. Symbols, Units, and Default Parameters

Symbol	Description	Default Value and Units
A	Rheological preexponent (dislocation)	$MPa^{-n}\ s^{-1}$
B	Rheological preexponent (diffusion)	MPa^{-1}
E	Activation energy	500 (ds), 300 (df) kJ/mol
V	Activation volume	10(ds), 6(df) cm^3/mol
g	Gravitational acceleration	9.8 m/s^2
h	Model height	660 km
C_p	Thermal capacity	1250 $J\ kg^{-1}\ K^{-1}$
n	Rheological power law exponent	3.5 (ds), 1 (df)
P	Deviatoric pressure	Pa
R	Gas constant	8.3 J/mol
Ra	Thermal Rayleigh number	4.43×10^6
Rb	Compositional Rayleigh number[a]	1.69×10^7, 1.48×10^6
T	Temperature	°C
T_s	Surface temperature	273 K
ΔT	Temperature drop over model domain	1350°C
T_p	Maximum plume excess temperature	250°C
R_p	Plume radius	50 km
$\acute{\varepsilon}$	Strain rate	s^{-1}
α	Thermal expansion coefficient	$3.5 \times 10^{-5}\ K^{-1}$
η_0	Reference viscosity	10^{20} Pa s
η	Viscosity	Pa s
κ	Thermal diffusivity	$10^{-6}\ m^2/s$
ρ	Mantle density	3300 kg/m^3
$\Delta\rho_1$	Density difference of upper crust and mantle	600 kg/m^3
$\Delta\rho_2$	Maximum density change due to depletion	52.5 kg/m^3
Q_0	Radioactive heating	0.04 $\mu W/m^3$
C_i	Composition field	0–1
C_η	Rheologically effective composition value[b]	0.6
$\Delta\eta_0$	Strengthening factor when $C \geq C_\eta$	

[a] 1.69×10^7 and 1.48×10^6 are the compositional Rayleigh numbers for crust and cratonic root, respectively.
[b] C_η is chosen to make the second cratonic layer has the maximum strengthening factor due to its initial compositional field.

$$Ra = \frac{\alpha \rho_0 g \Delta T h^3}{\kappa \eta_0} \tag{4}$$

$$Rb_i = \frac{\delta \rho_i g h^3}{\kappa \eta_0} \tag{5}$$

$$Di = \frac{\alpha g h}{C_p} \tag{6}$$

A particle-tracking technique is used to track different chemical materials [*Van Hunen et al.*, 2000; *Di Giuseppe et al.*, 2008], which has been benchmarked against *Van Keken et al.* [1997] and *Schmeling et al.* [2008]. The following compositional equation is thus solved:

$$\frac{\partial C_i}{\partial t} + (\mathbf{u} \cdot \nabla) C_i = 0 \tag{7}$$

Two particle functions are used in our models, with $i = 1$ and 2 representing the crust and the depleted mantle, respectively. As non-Newtonian rheology has been found to be important for both the stability and dynamics of the cratonic lithosphere [*Wang et al.*, 2014; *Wang et al.*, 2015], we use a composite rheology of non-Newtonian and Newtonian rheology to represent the dislocation creep and diffusion creep, respectively. Thus, the composition-dependent viscosities are calculated as follows:

$$\eta_{dl} = A^{\left(-\frac{1}{n}\right)} \dot{\varepsilon}^{\left(\frac{1-n}{n}\right)} exp\left(\frac{E + \rho g z V}{nRT}\right) \times \Delta\eta \tag{8}$$

$$\eta_{df} = B exp\left(\frac{E + \rho g z V}{RT}\right) \times \Delta\eta^n \tag{9}$$

$$\eta_{eff} = min(\eta_{dl}, \eta_{df}) \tag{10}$$

The implementation of non-Newtonian rheology has been benchmarked against *Christensen* [1984]. Due to the nonlinear stress-strain rate relationship used in the composite rheology, the effective compositional

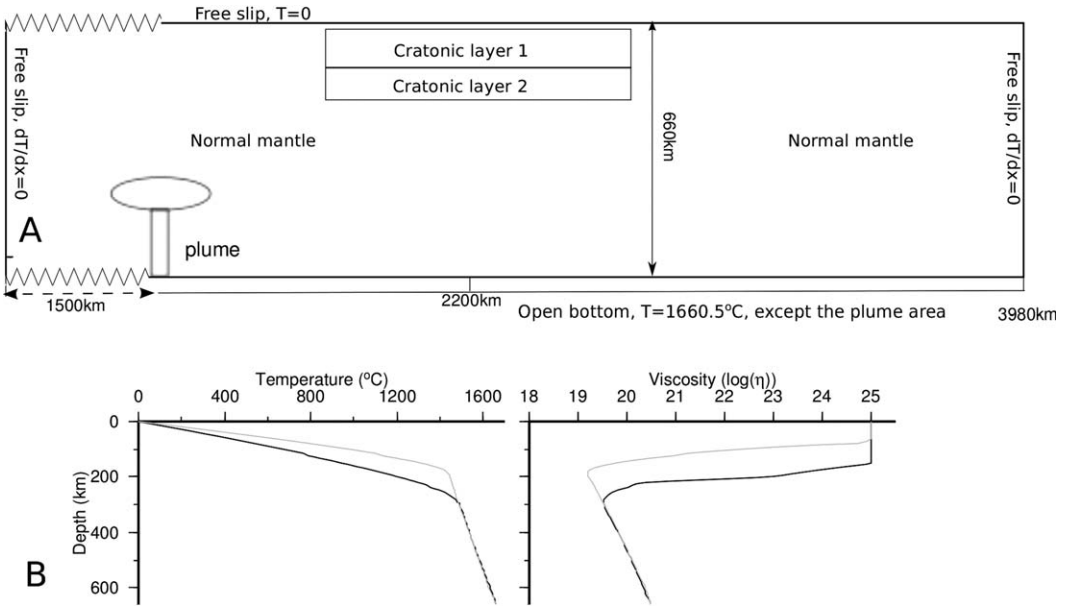

Figure 1. (a) Model setup, including the initial chemical layers of cratonic root, mechanical thermal boundary condition, and plume locations. (b, left) Typical geotherms and (right) effective viscosity profile of cratonic (black) and normal lithosphere (gray) as the initial thermal condition.

viscosity increase depends on the ambient stress or strain rate, and two end member situations exist. For the hypothetical case that strain rate is kept constant, changing the strengthening factor $\Delta\eta$ in equation (8) will change the effective viscosity proportionally. If, however, stress remains constant, then increasing $\Delta\eta$ will result in an effective viscosity increase of $\Delta\eta^n$. In this study, we report "constant strain rate" values $\Delta\eta$ in equation (8) and values used ($\Delta\eta = 2, 3, 4, 5, 6$) actually lead to an increase of non-Newtonian viscosity by $\Delta\eta^n = 11.3, 46.8, 128, 279.5$, and 529.1 in the definition of "constant stress." Thus, we use a strengthening factor of $\Delta\eta^n$ for Newtonian viscosity in equation (9) to have similar compositional effect. Considering the significant variation in the results of the laboratory experiment on mantle rheology [*Hirth and Kohlstedt*, 1996; *Karato*, 2010; *Fei et al*., 2013], the range of strengthening factors in this study is considered representative.

2.2. Model Setup

The computational domain is 660 km deep and 3980 km wide, with mantle plumes rising up on the left side of the thick chemical root (hereafter referred to as the "craton"). This model setup is illustrated in Figure 1a together with the mechanical and thermal boundary conditions. We calculated a model with a stable chemical root (with compositional buoyancy and strengthening factor of $\Delta\rho = 31.5$ kg/m^3 and $\Delta\eta = 4$, respectively) to a quasi-steady state thermal condition and use it as the initial temperature field in this study. Typical thermal and viscosity profiles for cratonic and normal lithosphere are displayed in Figures 1b and 1c.

A two-layer chemical root is used, with the following characteristics for all the cases in the parametric study (section 3): (1) a highly depleted layer from 36 km (Moho) to 150 km depth in which the chemical value decrease from 1 to C_η; (2) a less depleted layer from 150 to 200 km with constant chemical value C_η. To avoid the sharp transition between chemical root and asthenosphere, a 20 km thick buffer layer is added underneath the chemical root in which the chemical value gradually decreases to 0. Thus, an initial chemical root of 200–220 km is setup in our models. The composition value C tracked with tracers controls both the buoyancy and strengthening of continental root through

$$\rho_c = \rho_m - C_i \Delta\rho_i \tag{11}$$

$$\Delta\eta = \Delta\eta_0^{\,min\left(1,\frac{C_2}{C_\eta}\right)} \tag{12}$$

Because the two chemical layers in all calculations have initial compositional values larger than or equal to C_η, the initial strengthening factor of the whole root is always $\Delta\eta_0$ in equations (8–10). Any reasonable

buoyancy variation of the first chemical layer is found to have little effect on the dynamics. So we focus on the compositional buoyancy ($\Delta\rho$) and strengthening factor ($\Delta\eta$) of the second layer to explore the effects of metasomatic refertilization on the depleted continental lithosphere. The density reduction due to a bulk rock Mg number (Mg#) change from fertile mantle (with Mg# $\sim$ 88) to depleted cratonic root (Mg# = 92–94) is found to be $\sim$1.5–2.5% [*Schutt and Lesher*, 2010]. As the second layer is less depleted, we use a reduced density of 3258 kg/m^3 (density reduction of 42 kg/m^3 or 1.27% of the reference mantle density of 3300 kg/m^3) to represent the maximum effect of mantle depletion on the density of lithosphere root. In order to quantitatively monitor the lithosphere thickness changes caused by the convective erosion, we define a thermal lithosphere-asthenosphere boundary (LAB) by the isotherm of $T = 1325^\circ$C and calculate the average thicknesses of the specific area through time.

Mantle plumes are generated through a basal Gaussian thermal anomaly with excess potential temperature T_p and radius R_p [*Zhong and Watts*, 2002], centered at $x = 1500$ km (unless stated otherwise) (Figure 1a). An open flow boundary condition is used at the bottom, so the thermal plume would rise up where the thermal anomaly is located. The instantaneous nondimensional plume flux F_p is calculated at every time step as

$$F_p = \int V_z \cdot dT ds \tag{13}$$

while the total plume inflow (F_{total}) is monitored using

$$F_{total} = \int F_p dt \tag{14}$$

where V_z and dT are the vertical velocity and excess temperature at the bottom, respectively. By controlling the location, radius, and total plume inflow of the Gaussian thermal anomaly, a variety of different plumes are set up for different models. The plume forms at an arbitrary time (30 Myr after the model start in most calculations) and ends automatically when the total plume inflow reaches a predefined threshold value. This procedure ensures the same total plume inflow for varying plume parameters such as the plume location or radius.

A total of 96-by-576 finite elements are used with mesh refinement near the root area, which provides a spatial resolution of 4.5 km per element for the root area and 8–9 km per element elsewhere. A total number of $>$2.5 million tracers are randomly distributed in the domain at the beginning of the computation, which provides an average tracer density of 47 tracers per element. In order to handle the tracer inflow and outflow, tracers at the elements facing any open boundaries are refreshed at every time step. Thus, the total number of tracers in the computation domain is statistically constant.

3. Plume-Root Interaction

We first illustrate how the plume impacts and erodes thick continental lithosphere through temperature, buoyancy, chemical, and viscosity evolution. Then the effects of different root buoyancy and strength are explored by monitoring the erosion of the root in different models. We also compare these models with those without any plumes to understand the actual effects of plume impact. Afterward, the effects of different plume setups are investigated.

3.1. Plume Impact on the Subcratonic Root

Figure 2a illustrates how a plume rises up near the edge of a craton and impacts on the thick continental root. Figures 2b–2e show the temperature, buoyancy, and viscosity images of four time snapshots when a plume impinges on the thick root in the enlarged area indicated in Figure 2a. The changing chemical root shape through time (Figures 2b–2e) illustrates that the main impact and erosion focuses on the edge of the root whereas the top layer of the root shows little effect from the dynamics of plume impact. Therefore, we only further explore the effects of the compositional buoyancy ($\Delta\rho$) and the strengthening factor ($\Delta\eta$) of the lower cratonic layer on the erosional behavior of the root in the early stage. The root setup in Figure 2 is characterized by $\Delta\rho = 21$ kg/m^3, $\Delta\eta = 3$ of the second layer, which is further explained in section 3.2. For other model calculations with different $\Delta\rho$ and $\Delta\eta$ (see below), the dynamical details might vary, but the general deformation pattern as shown in Figure 2 still applies.

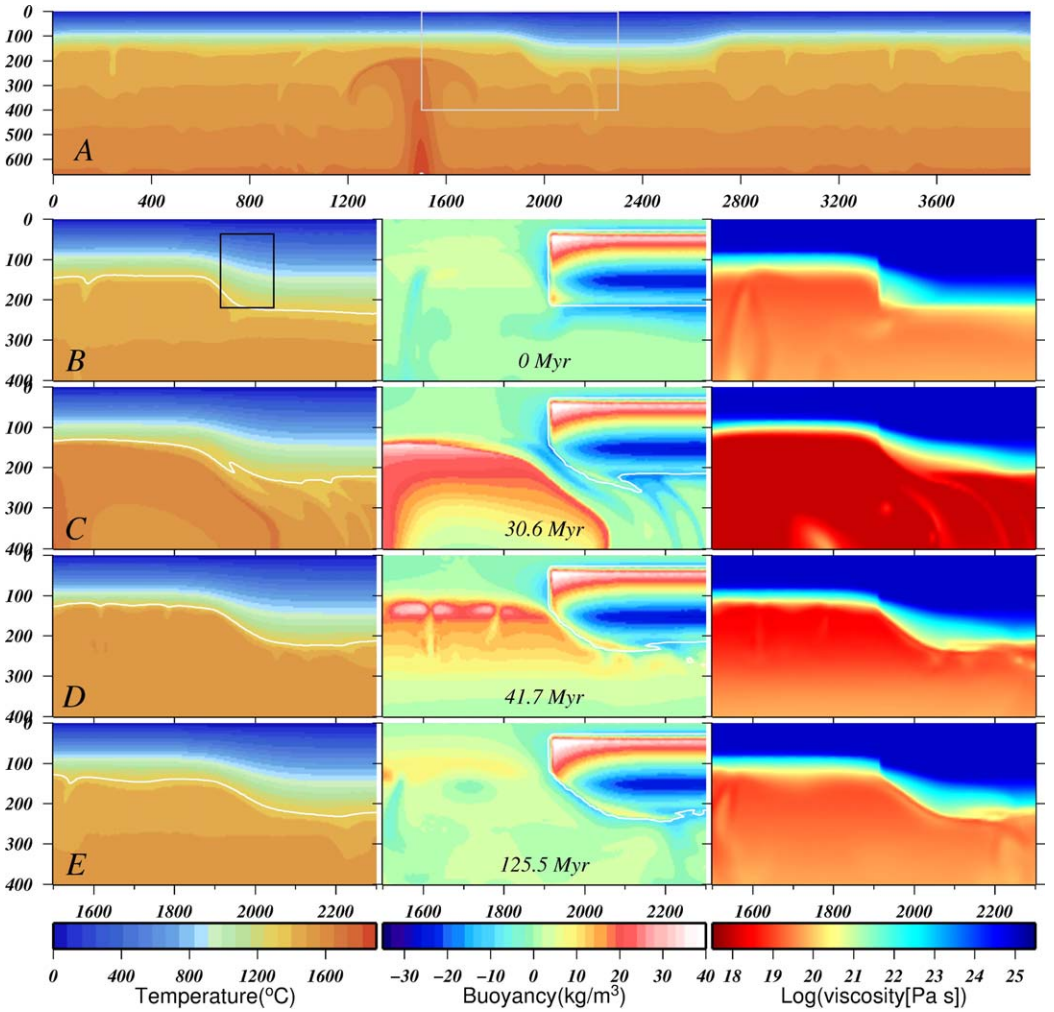

Figure 2. (a) Temperature distribution when a plume rises up near the thick continental root. The gray box indicates the zoomed area in Figures 2b–2e to focus on the erosion of continental root by the plume-induced flow. (left) The temperature, (middle) buoyancy, and (right) effective viscosity of a model in which a plume (30 Myr) impacts the thick root, with four time snapshots at (b) 0 Myr, (c) 30.6 Myr, (d) 41.7 Myr, and (e) 125.5 Myr. The chemical boundary of the root is outlined by the white line in the buoyancy field that is the defined by the $C = 0.1$ contour. The black box in Figure 2b specifies the area of the left root edge where the erosion is monitored. This model has $\Delta\rho = 21$ kg/m^3; $\Delta\eta = 3$. The buoyancy field is calculated relative to a reference density profile based on the average geotherm of normal lithosphere before the plume arrival.

The buoyancy field has a strong vertical stratigraphy and the peak negative buoyancy is at a depth near the LAB of normal lithosphere (middle in Figures 2b–2e). This structure is dependent on the chemical layer setup and the thermal structure of both two types of lithosphere. The uppermost root is frozen by its positive or neutral buoyancy and high viscosity ($>10^{24}$ Pa s, Figures 2b–2e), and it has little effect on the dynamics. The deeper root area, that contains the maximum negative buoyancy, is also protected by its high viscosity ($>10^{23}$ Pa s) as it is located in the interior of the root (Figures 2b–2e). The lowermost root is almost neutrally buoyant because the negative thermal buoyancy of the root decreases with depth. As it falls into the rheologically active area, the lowermost root is the most susceptible part to dynamical removal, especially in the peripheral area.

When the buoyant plume material arrives and ponds nearby, the lower part of cratonic root becomes gravitationally more unstable and strongly sheared by the plume-induced flow (Figures 2c and 2d). Due to the non-Newtonian rheology (equation (8)), the shearing of plume flow reduces the viscosity of the root edge significantly (Figure 2c), which allows instantaneous erosion. However, the compositional buoyancy and strengthening of the root interior prevents the development of a significant gravitational instability such as described by *Houseman and Molnar* [1997] and only the root material at edge of the root is sheared and eroded away. After the major plume impact, small-scale convection dominates the underside of the normal, noncratonic lithosphere, which also propagates to the edge of the cratonic root and causes further local

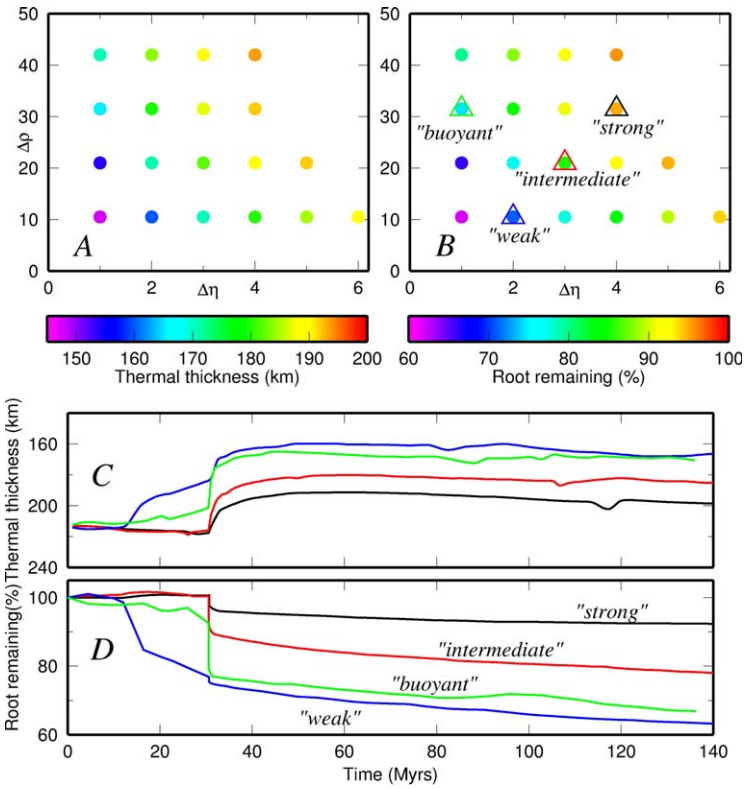

Figure 3. Effects of root chemical buoyancy and rheology on its erosion. (a) The average thermal lithospheric thickness (defined as the $T = 1325°C$ isotherm) and (b) remaining chemical root percentage (in terms of geometrical volume) of the left root edge (1914–2046 km) at 50 Myr. (c) Evolution of average thermal thickness and (d) chemical root remaining through time. Each line represents one of the models with a colored triangle in Figure 3b: a "strong" root (black, $\Delta\rho = 31.5$ kg/m^3; $\Delta\eta = 4$), an "intermediate" root (red, $\Delta\rho = 21$ kg/m^3; $\Delta\eta = 3$), a "weak" root (blue, $\Delta\rho = 10.5$ kg/m^3; $\Delta\eta = 2$), and a "buoyant" root (green, $\Delta\rho = 31.5$ kg/m^3; $\Delta\eta = 1$).

erosion (Figure 2d). Once the plume-affected material has cooled down, the lower part of the root returns back to approximate neutral buoyancy (Figure 2e), in which thermal and compositional buoyancy cancel each other out.

3.2. Effects of Chemical Root: Buoyancy and Strength

The thermochemical erosion of a thick continental root by a plume is studied using two observables: the local geotherm and the removal of the chemical root material. Because a change in the thermal profile does not necessarily correspond directly to the removal of the chemical root, the following two physical quantities are calculated at each time step as monitors of the erosion: (1) the average thermal thickness; (2) the remaining chemical root as a percentage of its original volume. Since the main erosion takes place at the edge of the root, we monitor the erosion of the left root edge between $x = 1914$ km and $x = 2046$ km as illustrated by the black rectangular box in Figure 2b.

Figure 3 shows the average thickness (a) and remaining root percentage (b) for the left edge of the root at 50 Myr (i.e., 20 Myr after the plume event) for 19 models with different root setups. Both of the two erosion monitors demonstrate that the erosive strength of the plume on the root strongly depends on the chemical buoyancy and strengthening of the root: more buoyant and stronger chemical roots experience less erosion. A "strong" root model ($\Delta\rho = 31.5$ kg/m^3, $\Delta\eta = 4$) shows very limited erosion ($\sim$5%), while an "intermediate" root model (with $\Delta\rho = 21$ kg/m^3, $\Delta\eta = 3$) shows some degree of erosion ($\sim$15%). By either reducing the buoyancy (to $\Delta\rho \leq 10$ kg/m^3) or the strengthening factor (such as in the "buoyant" root model with $\Delta\rho = 31.5$ kg/m^3, $\Delta\eta = 1$), the erosion of the root edge would increase substantially. If both the buoyancy and strengthening factor are reduced, such as in a "weak" root model, very significant erosion ($>$30%) occurs (Figures 3a and 3b).

Four root models ("strong," "intermediate," "weak," and "buoyant") as defined in Figure 3b are selected to demonstrate the evolution of the left craton root edge through time in Figures 3c and 3d. The impact of

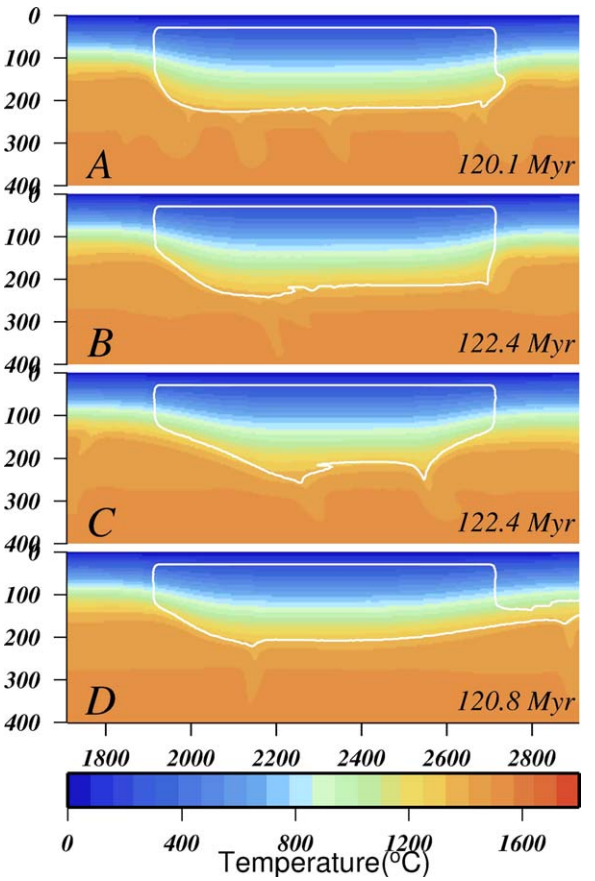

Figure 4. The temperature field and chemical root shape at around 120 Myr for four models. The models with a (a) "strong," (b) "intermediate," (c) "weak," and (d) "buoyant" root.

the plume arrivals around 30 Myr is clearly indicated by sudden changes of the curves in Figures 3c and 3d. After the main plume impact, the average thermal lithosphere thickness grows slowly as the mantle cools down (Figure 3c), while the erosion of the "chemical" root might still continue (as in most models) or slow down significantly (such as in the "strong" root model) in Figure 3d. The shape of chemical roots and thermal structures at around 120 Myr of these four models is shown in Figure 4. Models with the "strong" and "intermediate" root only demonstrate local changes of the root edges by the plume impact (Figures 4a and 4b), while there are more widespread erosion effects in the other models (Figures 4c and 4d).

To separate the effects of a plume impact from normal plate-mantle interaction, we also calculate three nonplume models with "strong," "intermediate," and "weak" roots and monitor the chemical root remaining for the left edge and the whole root for a much longer period of 1 Gyr (Figure 5a). The thermal thickness is not monitored as it is affected significantly by cooling of the lithosphere over such a long period. The "strong" root maintained a well-shaped root (Figure 5b) with 99% of the original root still present. The "intermediate" strength root also survived with 92% of the root intact, albeit with significant erosion (Figure 5c) at the edges. The "weak" root, however, almost completely loses its lower part after 1 Gyr with 65% and 75% of the root remaining for the left edge and the whole root, respectively. This implies that such a "weak" root would essentially not survive since its formation in Archean or Proterozoic times until today. Comparison of the erosion at the left craton edge between models with and without plume impact shows that the short-term erosion with plume impact is quite similar to the long-term erosion without plumes: 92.5 versus 92.8% for the "strong" root, 79.5% versus 76.4% for the "intermediate" root.

All these results demonstrate that the compositional buoyancy and strengthening of the cratonic root plays a significant role in mantle dynamics in which a plume impinges on a thick continental lithosphere. A well-preserved root seems to be characterized by being "strong" ($\Delta\rho$ =31.5 kg/m^3 and $\Delta\eta = 4$), and under such conditions, the plume impact does not erode the root very much. While a less buoyant and viscous root ("intermediate" root with $\Delta\rho = 21$ kg/m^3, $\Delta\eta = 3$) shows significant erosion of its edge by a plume impact, the overall fractional erosion is similar to that which would occur over 1 Gyr of plate-mantle interaction without any plume impact. An even less buoyant and viscous root ("weak" root with $\Delta\rho = 10.5$ kg/m^3, $\Delta\eta = 2$) will not be able to survive at all, with or without a plume impact. Therefore, the effect of the plume impact is to speed up the erosion significantly over a short period (from hundreds to tens of Myr), but it does not necessarily induce extra erosion in the long term. This agrees well with craton stability results presented by *Sleep* [2003].

3.3. Influence of Plume Characteristics

The effects of different plume setups are explored in this section. The temporal evolution of the average thermal thickness and fraction of chemical root remaining at the root edge is shown in Figure 6. The "intermediate" root ($\Delta\rho = 21$ kg/m^3, $\Delta\eta = 3$) is applied in all models in this section and the default plume setup

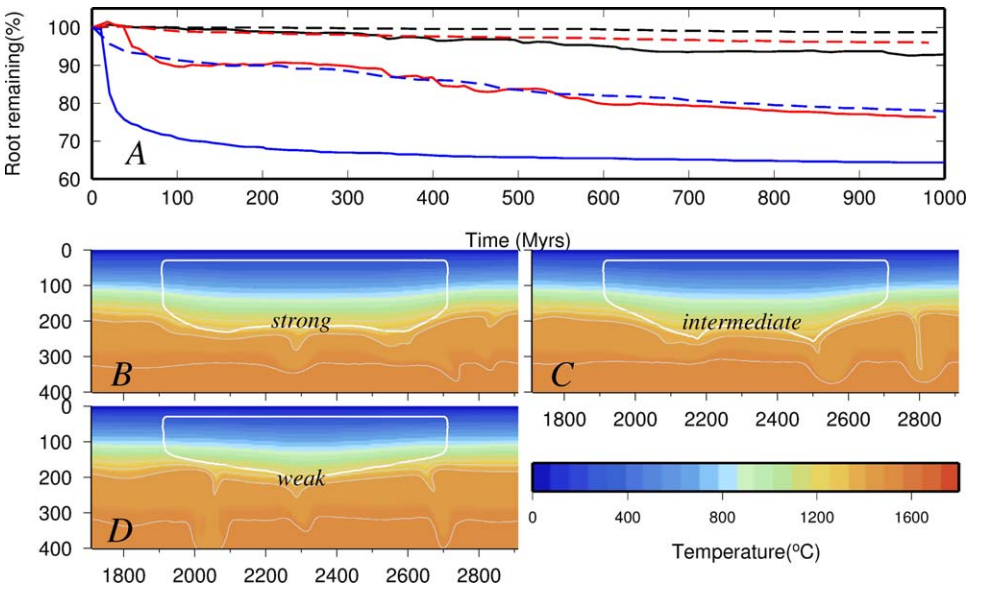

Figure 5. Results for three long duration models without a plume impact. (a) The evolution of the chemical root remains for 1 Gyr for the "strong" root (black), "intermediate" root (red); and "weak" root (blue). The solid lines show the change of the root remains for the left root edge, while the dashed lines show the result for the whole root. The temperature field and root shape at 1 Gyr for the models with (b) "strong," (c) "intermediate," and (d) "weak" root.

in previous models is used as the reference. A model with total plume inflow $F_{total} = 0$ (equation (14)) shows that the root edge would still experience some erosion without any plume impact. But the total erosion after 200 Myr (i.e., a relatively long period in comparison to a typical plume impact duration) is significantly smaller than the rapid erosion in the reference model with a plume impact. Compared to the reference model, the model with half of the total plume inflow shows much less erosion through both the average thermal thickness and chemical root remaining in Figures 6a and 6b. However, by doubling the total plume inflow, the erosion of the root edge increases only marginally (Figure 6b), although the average thickness shows a clear difference (Figure 6a). Therefore, a certain critical amount of plume flux is required to erode the thick chemical root substantially and quickly, but increasing the total plume inflow beyond this critical

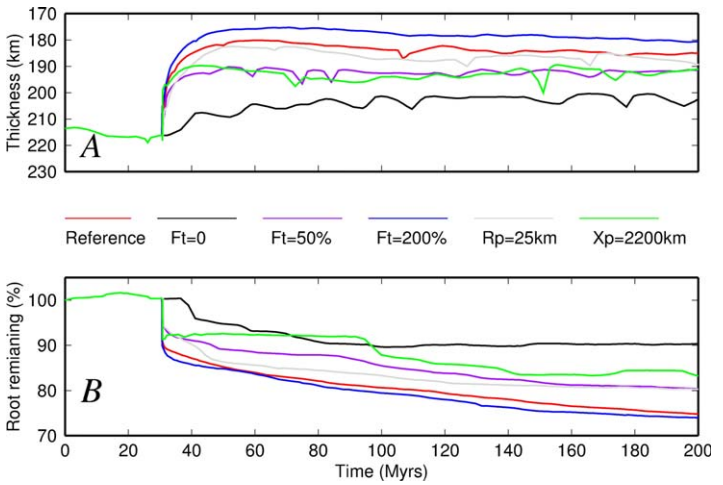

Figure 6. (a) The evolution of thermal thickness and (b) chemical root remains for models with different plume setups. F_t, R_p, and X_p are the total plume inflow (relative to the reference case), plume radius, and plume location, respectively. The reference model has $X_p = 1500$ km, $R_p = 50$ km, $F_t = 100\%$, while the every other model one of these parameters is changed as indicated. For $F_t = 0$, there is no plume event in the model. For other models, the plume is at the left side of chemical root when ($X_p = 1500$ km), except for $X_p = 2200$ km, in which case the plume is right underneath the root as shown in Figure 1a.

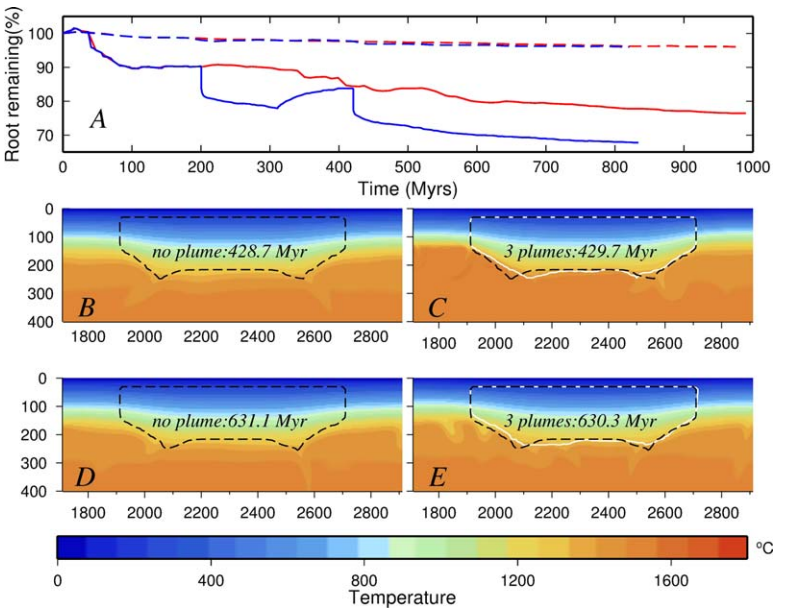

Figure 7. Results of multiple plumes experiment. (a) The evolution of chemical root remains for models with no plume (red) and three plumes (blue). The dashed lines show the evolution of the whole craton, while the solid lines show the evolution for the left root edge. The three plumes are 200 Myr at $x = 1500$ km, 310 Myr at $x = 3000$ km, and 420 Myr at 1500 km. (b and d) Temperature field and root shapes (dashed lines) in the model without any plume impact at around 430 and 630 Myr. (c and e) Temperature field and root shapes (white lines) in the model with three plumes at around 430 and 630 Myr. The root shapes in Figures 7b an 7d are also plotted as dashed line for comparison in Figures 7c and 7e, respectively.

level does not necessarily induce significantly more erosion of the chemical root if the compositional buoyancy and strengthening are unaltered. A model with a much smaller plume radius (25 km) also makes some difference. As the same total plume inflow is applied (i.e., the smaller plume remains active for longer), the change in thermal thickness of the root edge is comparable to the reference model (Figure 6a), but the erosion of the chemical root decreases substantially (Figure 6b). However, no obvious increase is found when an even larger plume radius is applied (not shown). This means that the instantaneous removal of the chemical root by plume impact depends on the vigor of the plume-induced flow, but a threshold value of plume vigor is required for the impact to be significant.

A model with the plume rising up directly underneath the root ($x = 2200$ km) does not show an increase of erosion (Figures 6a and 6b). On the contrary, the average thermal thickness is similar to the model with half of the total plume inflow (Figure 6a). This rather counterintuitive result can be explained by the fact that the impact of plume flow on the root is weaker when it flows from the thick lithosphere to the thin lithosphere and encounters less resistance. Such an impact would cause similar erosion at the right root edge which is not monitored in Figure 6. However, the impact of the plume directly underneath the root is still distinguished, as the root remaining in Figure 6b shows a small increase after the main decrease at 30 Myr. This change is due to the transition of the flow direction near the root area during the plume impact.

Figure 7 compares the long duration model in section 3.2 with a model in which a series of three plumes impacts the subcratonic root sideways, with plume number 1 and 3 positioned at $x = 1500$ km and plume number 2 at the other side of the craton at $x = 3000$ km, each with the intensity of the reference plume above. The chemical portion of the whole cratonic root is not evenly affected by the three plume impacts, though the root edge shows a clear change corresponding to every plume impact (Figure 7a). The slight increase in size of the chemical root remaining at the left-side root edge indicates that plume number 2 transports root material in the direction of plume driven flow. The comparison between Figures 7b, 7d and 7c, 7e demonstrates that the most recent plume impact erodes and deforms the chemical root to some extent, but the long-term plate-mantle interaction would overwrite this effect. Therefore, this comparison further confirms the very limited effect on the cratonic lithosphere of thermomechanical erosion by mantle plumes.

4. Discussion

4.1. Effect of Plume Impact on Thick Continental Lithosphere

Our modeling results illustrate that plume arrival beneath cratonic mantle has two main effects: (1) due to the stress-dependent rheology, the arrival of a strong plume-induced mantle flow deforms and weakens the continental root, especially at the root edges; (2) the hot, buoyant plume material increases the vigor of the thermochemical convection surrounding the root and causes further erosion. However, only relatively strong cratonic lithosphere would have survived since its creation in the Archean or Proterozoic. For such cratons, mechanical erosion caused by a nearby plume would be rather limited, unless the chemical root has been recently weakened. Thus, according to our results, a mantle plume is unlikely to cause short-time scale (tens of Myr) mechanical erosion of an unweakened ancient cratonic root.

Plume-craton interaction is likely to be more complicated than our (by definition simple) model calculations suggest. Plume-induced mantle depletion is not included in our models, but it might actually inhibit the thermal erosion of the root once a layer of depleted material formed at the base [*Manglik and Christensen*, 1997]. Plumes in a three-dimensional (3-D) dynamic situation might exhibit different behavior compared with two-dimensional (2-D) models [*Ribe and Christensen*, 1994; *Van Keken and Gable*, 1995]. However, mechanical plume erosion is not expected to be more efficient in 3-D as the plume vigor would reduce with distance from the plume stem, and the 3-D situation might require a more proximal plume in order to have a substantial influence on the cratonic root. Our models agree with previous work showing that a plume can reduce the width of a cratonic root [*Sleep et al*., 2002], but they also indicate that this reduction would be rather limited for classic cratonic roots that have already survived since the Archean. The impact of a plume on a cratonic root might be stronger if widespread melts are induced by a craton-centered plume and lead to metasomatic weakening. Also the advective transport of heat by melts that penetrates the lithosphere is not included in our models and is likely to be more efficient than the thermal conduction alone at the base of lithosphere. The effects of such plume metasomatism require further geodynamic investigation with interactive feedback between melt extraction and metasomatic weakening.

4.2. Metasomatic Weakening

Rapid, significant removal of thick continental lithosphere that previously survived billions of years of Earth's dynamic history is only likely to happen if the compositional buoyancy and strengthening of large fractions of the root are significantly altered somehow. While the thick lithospheric "lid" provided by cratonic roots limits adiabatic melting compared to that seen in shallower lithosphere, it is clear that silicate melt metasomatism strongly affects lithospheric mantle, even at the base of $>$150 km thick cratons [e.g., *Smith and Boyd*, 1992]. By refertilization and enrichment in garnet and/or clinopyroxene, the compositional buoyancy of originally depleted cratonic root could be removed. Carbonate-rich low degree melts generated at 6 GPa will infuse the lowermost cratonic lithosphere with phlogopite mica and carbonate [e.g., *Foley*, 2011]. Such water-rich melts add water both bound to metasomatic phlogopite and by diffusion into olivine. Besides weakening the lithosphere by adding water [*Peslier et al*., 2012], any melt-rock interaction during the process of metasomatism could also have a substantial weakening effect on the rheology of the refractory continental root [*Foley*, 2008; *Holtzman et al*., 2012], especially for local melt accumulation. Hence, even though we do not model the process and the rheological effects of metasomatism explicitly, the important geodynamical implications (i.e., a buoyancy and rheological weakening) of metasomatic refertilization on the stability of thick continental root [*Foley*, 2008; *Lee et al*., 2011; *Tang et al*., 2013] are manifest in our models.

Our results also show that, for the lower part of the root, there is a range of realistic cratonic compositional buoyancies (21 kg/m^3 $< \Delta\rho <$ 42 kg/m^3) and rheological strengthening ($\Delta\eta \geq 3$), within which the thick root is not significantly affected by the mechanical erosion of mantle plumes. This suggests that a low degree of metasomatism does not necessarily change the dynamical stability of the whole continental root. As cratonic mantle is not found to be compositionally refertilized significantly on average [*Rudnick et al*., 1998; *Pearson and Nowell*, 2002], this finding may explain why many cratonic roots are still extant, even though they might be metasomatized locally to some degree during their secular evolution. Kimberlite pipes and other small-degree melts that sample the lower parts of the lithospheric mantle only provide small local snapshots of the cratonic root at specific points in time. More detailed, widespread studies of the distribution, extent, and effects of metasomatism on cratonic roots are required to fully understand the geodynamical implications of metasomatic refertilization. Nonetheless, it is clear that the extent of lithospheric

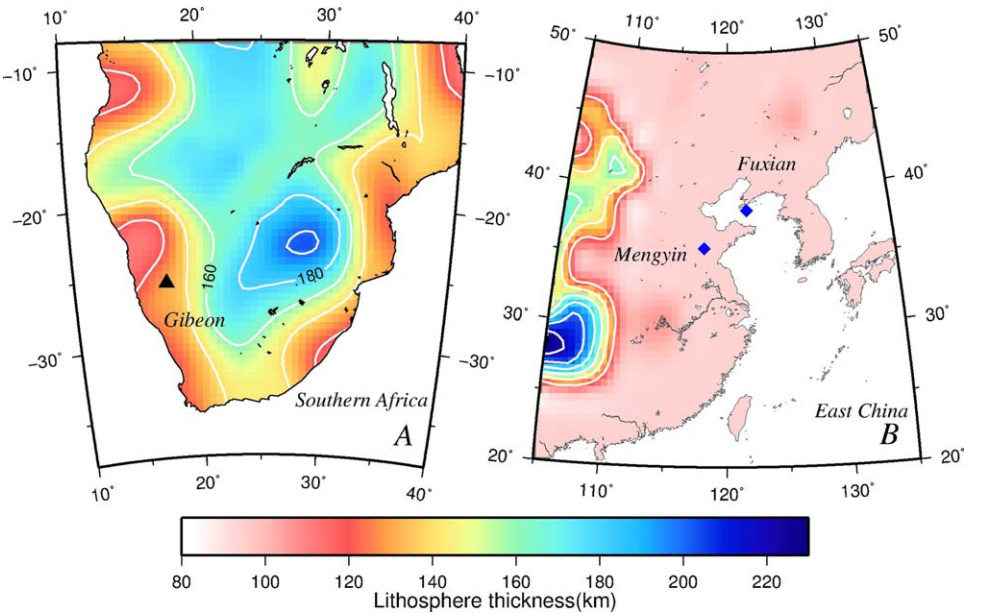

Figure 8. Comparison of current thicknesses from global seismic study [*Priestley and McKenzie*, 2013] and paleo-thickness from kimberlites at southern Africa [*Mather et al*., 2011] and the North China Craton [*Menzies et al*., 1993].

weakening that occurs via high-pressure infiltration of carbonate-silicate melts at the base of the cratonic mantle depends on the intensity and spatial extent of the metasomatic events.

4.3. Global Implications

As discussed above, our numerical models clearly demonstrate the effects of both plume impact and metasomatic refertilization on the erosion of the subcontinental lithosphere during mantle thermal events. The models thus may have important implications for continental dynamics, including the cause of continental breakup and lithosphere thinning. Lithosphere thinning has been suggested for a number of Precambrian terranes [*Lee et al*., 2011], and here we choose thinning of the lithosphere underneath Gibeon, southern Africa, the destruction of North China Craton (NCC) and the breakup of the North Atlantic Craton as three examples that highlight the global relevance of the presented numerical model results.

4.3.1. Lithosphere Thinning Beneath Southern Africa

Kimberlite-derived mantle xenoliths show that the Proterozoic lithosphere underneath Gibeon, Namibia in southern Africa used to have a similar geotherm to the Kaapvaal craton at 70 Ma, which indicates a lithosphere thinning of 40–50 km to reach the current lithosphere thickness (Figure 8a) of this area [*Bell et al*., 2003; *Boyd et al*., 2004; *Mather et al*., 2011; *Priestley and McKenzie*, 2013]. Given the multiple plume tracks across southern Africa starting at 44 Ma [*O'Connor et al*., 2012], lithospheric thinning by mantle plume erosion seems to be a good candidate for this thinning event. However, according to our model results, a rather sudden significant thinning of this lithosphere after its long-term survival since Proterozoic times [*Pearson et al*., 2004] until at least 70 Ma requires a substantial, recent weakening event. This indicates that some metasomatic weakening must have occurred relatively shortly before or during the plume arrival. Multistage metasomatism has indeed been documented since 170 Ma, including the Group I (108–74 Ma) and Group II (143—117 Ma) kimberlite eruptions [*Konzett et al*., 1998; *Griffin et al*., 2003a; *Becker and Le Roex*, 2006; *Gibson et al*., 2008; *Kobussen et al*., 2008]. Therefore, we conclude that these documented metasomatism events must have played a very important role in the weakening of the lithosphere mantle, while the recent plume events may help the thinning to occur rapidly after the weakening.

4.3.2. Destruction of the North China Craton

The destruction of the eastern part of the North China Craton (NCC) has attracted a lot of attention as the only undisputed example of the almost complete removal of the cratonic root [*Zhu and Zheng*, 2009]. The dramatic loss of $>$120 km of lithosphere was first demonstrated by *Menzies et al*. [1993] who noted the difference in equilibration depths given by deeply derived garnet-peridotites from Ordovician kimberlites

versus the shallow depth of lithosphere in the Cenozoic indicated by spinel peridotites erupted by alkali basalts. The shallow present-day lithospheric thickness is confirmed by seismic topography (Figure 8b). The survival of this cratonic root from the Archean to the Mesozoic suggests an initially strong cratonic root that could resist long-term thermomechanical erosion by interaction with the mantle. Our model results suggest that the relatively sudden removal of this cratonic root requires a recent, significant weakening of more than perhaps 100 km cratonic lithosphere. This unusual requirement has also been suggested by the geodynamic modeling of subduction-related convective erosion of the NCC [*He et al*., 2014]. A dehydrating stagnant slab underneath east Asia has been suggested to initiate the upwelling of "wet plumes" [*Richard and Iwamori*, 2010] or the formation of a large mantle wedge [*Zhao et al*., 2009; *He et al*., 2014]. A recent find of hydrous ringwoodite trapped in diamond [*Pearson et al*., 2014] confirms the enhanced water-carrying capacity of the transition zone. In this scenario, water originating from stagnant slabs in the transition zone that are heating up acts to lowers the solidus of mantle rocks, producing large amount of melts that metasomatize the cratonic root through fluid/melt-rock interaction (hydrous metasomatism) [*Niu et al*., 2005]. In addition, water or hydrous fluid at the subduction zone might also can trigger the eclogitization of the lower crust [*Jackson et al*., 2004; *Krystopowicz and Currie*, 2013] and provide the negative buoyancy required for foundering of the lower crust as well as the mantle lithosphere underneath [*Gao et al*., 2002; *Yu et al*., 2012]. The gravitational instability of the chemically buoyant lithosphere [*Jaupart et al*., 2007; *Wang et al*., 2015] provides a supportive mechanism of the destruction of the NCC. *Wang et al*. [2015] demonstrated the feasibility of episodic and multistaged gravitational instabilities of the weakened cratonic lithosphere consistent with the episodic magmatism/volcanism events of the NCC in the Mesozoic and Cenozoic. We note that, regardless of the exact mechanism, significant weakening by hydrous metasomatism and related processes must have played an essential role in the sudden destruction of the NCC and is consistent with our model results that emphasize the role of metasomatic weakening.

4.3.3. Rifting of the North Atlantic Craton and Opening of the Labrador Sea

Our last example highlights the role played by exotic small-degree volatile-rich melts in weakening the base of cratonic mantle over an extended time period prior to full-scale continental rifting. The continental breakup phase during the supercontinent cycle is often linked to plume impingement [*Hill*, 1991; *Anderson*, 1994; *Courtillot et al*., 1999; *Li and Zhong*, 2009; *Brune et al*., 2013; *Yoshida*, 2013]. *Brune et al*. [2013] studied the thermal and mechanical influence of a plume on 3-D continent breakup and found that a plume would reduce the strength of continents by several TN/m if tens of kilometers of lithosphere are eroded from the base of the continental lithosphere. Continental root erosion by mantle plumes without weakening of the originally stable lithosphere, however, is found to be very limited according to our modeling results. But (potentially plume-generated) melt weakening effects in the lithosphere assist the process of continental rifting [*Buck*, 2006; *Schmeling and Wallner*, 2012]. The North Atlantic Craton, exposed on the W and E sides of the Labrador Sea was rifted apart between 60 and 55 Ma, accompanied by the eruption of flood basalts. Prior to this, the cratonic root experienced a protracted history of metasomatic weakening that began with the eruption of Mesoproterozoic lamproites through deep ancient cratonic lithosphere followed by Neoproterozoic ultramafic lamprophyres in both Labrador and W. Greenland [*Tappe et al*., 2007, 2011]. This magmatism infused the lower lithosphere with carbonate and water at this time. Initially small-scale (∼30 km depth) lithosphere removal appears to have accompanied the eruption of alkalic melts during the Jurassic [*Tappe et al*., 2007], probably driven by small-scale convective flow whereas the arrival of a major plume at 60–55 Ma drove full-scale continental rifting of the metasomatically weakened lithosphere. This sequence of metasomatic weakening and thermomechanical erosion by small and large-scale mantle flow is aligned with our model results.

5. Conclusion

The hypothesis that a mantle plume might cause significant thinning of ancient, depleted continental mantle lithosphere is tested in our numerical models. The results show that the erosion caused by a plume impact on a strong continent (moderately strong and buoyant) is rather limited. Plumes impacting on less strong or less buoyant subcontinental roots produce significantly more erosion at root edges in a relatively short (approximately tens of Myr) amount of time. Without such a plume impact, a similar amount of erosion could eventually occur due to continued plate-mantle interaction, albeit over much longer time scales (several 100 Myr to 1 Gyr). Varying the plume radius, location, or total plume inflow does not significantly

change the effectiveness of the erosion. Instead, our modeling shows that generating a distinctly weakened root (less strong and less buoyant) is essential for significant thinning of subcontinental lithosphere over timescales of a few tens of Myr.

Fluid/melt-rock interaction during mantle metasomatism is probably the most likely mechanism to modify and weaken the depleted subcontinental lithosphere. Therefore, metasomatic weakening must have played an essential role on the thinning and reactivation of the originally stable subcontinental lithosphere, while the effect of any plume impact was to speed up the erosion and helped the removal of the lithospheric root to occur rapidly after the weakening. Depending on the extent of the metasomatic weakening, as well as the tectonic environment, different types of reactivation of the subcontinental lithosphere may occur, such as thinning of subcontinental lithosphere (e.g., underneath southern Africa), complete destruction of the cratonic root (e.g., at the NCC), and continental rifting (e.g., of the NAC). For the cases of southern Africa and the NAC, the documented plume activity may have enabled this process to occur rapidly. Other Precambrian terranes (e.g., the Colorado plateau and Wyoming craton) may have undergone similar processes, but more detailed studies of the distribution, extent, and effects of metasomatism might be needed to confirm this.

Acknowledgments

We thank Keith Priestley and Kathy Mather for kindly providing data and Mark Allen and Antoine Rozel for useful discussions. We also thoroughly appreciate the constructive reviews from Sally Gibson, Shijie Zhong and the (Associate) Editors. The data for this paper are available by contacting the corresponding author. The work has been supported by EU FP7 Marie Curie Initial Training Network "Topomod," contract 264517 (H.W.). J.v.H. acknowledges funding from the European Research Council (ERC StG 279828) and D.G.P. was supported by a Canada Excellence Research Chair.

References

Anderson, D. L. (1994), Superplumes or supercontinents?, *Geology*, *22*(4), 39–42.

Becker, M., and A. P. Le Roex (2006), Geochemistry of South African on- and off-craton, group I and group II kimberlites: Petrogenesis and source region evolution, *J. Petrol.*, *47*(4), 673–703, doi:10.1093/petrology/egi089.

Bell, D., M. Schmitz, and P. Janney (2003), Mesozoic thermal evolution of the southern African mantle lithosphere, *Lithos*, *71*(2–4), 273–287, doi:10.1016/S0024-4937(03)00117-8.

Boyd, F., D. G. Pearson, K. Hoal, and B. Hoal (2004), Garnet lherzolites from Louwrensia, Namibia: Bulk composition and P/T relations, *Lithos*, *77*, 573–592, doi:10.1016/j.lithos.2004.03.010.

Boyd, F. R. (1989), Compositional distinction between oceanic and cratonic lithosphere, *Earth Planet. Sci. Lett.*, *96*(1–2), 15–26, doi:10.1016/0012-821X(89)90120-9.

Brune, S., A. A. Popov, and S. V. Sobolev (2013), Quantifying the thermo-mechanical impact of plume arrival on continental break-up, *Tectonophysics*, *604*(3), 51–59, doi:10.1016/j.tecto.2013.02.009.

Buck, W. (2006), The role of magma in the development of the Afro-Arabian Rift System, *Geol. Soc. Spec. Publ.*, *259*, 43–54.

Carlson, R. W., A. J. Irving, D. J. Schulze, and B. C. Hearn Jr. (2004), Timing of Precambrian melt depletion and Phanerozoic refertilization events in the lithospheric mantle of the Wyoming Craton and adjacent Central Plains Orogen, *Lithos*, *77*(1–4), 453–472, doi:10.1016/j.lithos.2004.03.030.

Carlson, R. W., D. G. Pearson, and D. E. James (2005), Physical, chemical, and chronological characteristics of continental mantle, *Rev. Geophys.*, *43*, RG1001, doi:10.1029/2004RG000156.

Chesley, J., K. Righter, and J. Ruiz (2004), Large-scale mantle metasomatism: A Re-Os perspective, *Earth Planet. Sci. Lett.*, *219*(1–2), 49–60, doi:10.1016/S0012-821X(03)00698-8.

Christensen, U. (1984), Convection with pressure- and temperature-dependent non-Newtonian rheology, *Geophys. J. Int.*, *77*(2), 343–384, doi:10.1111/j.1365-246X.1984.tb01939.x.

Christensen, U., and D. Yuen (1985), Layered convection induced by phase transitions, *J. Geophys. Res.*, *90*(B12), 10,291–10,300.

Courtillot, V., C. Jaupart, I. Manighetti, P. Tapponnier, and J. Besse (1999), On causal links between flood basalts and continental breakup, *Earth Planet. Sci. Lett.*, *166*(3–4), 177–195, doi:10.1016/S0012-821X(98)00282-9.

Di Giuseppe, E., J. van Hunen, F. Funiciello, C. Faccenna, and D. Giardini (2008), Slab stiffness control of trench motion: Insights from numerical models, *Geochem. Geophys. Geosyst.*, *9*, Q020149, doi:10.1029/2007GC001776.

Doin, M.-P., L. Fleitout, and U. Christensen (1997), Mantle convection and stability of depleted and undepleted continental lithosphere, *J. Geophys. Res.*, *102*(B2), 2771–2787, doi:10.1029/96JB03271.

Ebinger, C., and N. Sleep (1998), Cenozoic magmatism throughout east Africa resulting from impact of a single plume, *Nature*, *395*, 788–791.

Fei, H., M. Wiedenbeck, D. Yamazaki, and T. Katsura (2013), Small effect of water on upper-mantle rheology based on silicon self-diffusion coefficients, *Nature*, *498*(7453), 213–215, doi:10.1038/nature12193.

Foley, S. F. (2008), Rejuvenation and erosion of the cratonic lithosphere, *Nat. Geosci.*, *1*(8), 503–510, doi:10.1038/ngeo261.

Foley, S. F. (2011), A reappraisal of redox melting in the Earth's mantle as a function of tectonic setting and time, *J. Petrol.*, *52*(7–8), 1363–1391, doi:10.1093/petrology/egq061.

François, T., E. Burov, B. Meyer, and P. Agard (2012), Surface topography as key constraint on thermo-rheological structure of stable cratons, *Tectonophysics*, *16*, 106–123, doi:10.1016/j.tecto.2012.10.009.

Gao, S., R. L. Rudnick, R. W. Carlson, W. F. McDonough, and Y.-S. Liu (2002), Re-Os evidence for replacement of ancient mantle lithosphere beneath the North China craton, *Earth Planet. Sci. Lett.*, *198*, 307–322.

Gibson, S. A., J. Malarkey, and J. A. Day (2008), Melt depletion and enrichment beneath the Western Kaapvaal Craton: Evidence from Finsch peridotite xenoliths, *J. Petrol.*, *49*(10), 1817–1852, doi:10.1093/petrology/egn048.

Gibson, S. A., S. C. McMahon, J. A. Day, and J. B. Dawson (2013), Highly refractory lithospheric mantle beneath the Tanzanian Craton: Evidence from Lashaine pre-metasomatic garnet-bearing peridotites, *J. Petrol.*, *54*(8), 1503–1546, doi:10.1093/petrology/egt020.

Griffin, W., S. O'Reilly, L. Natapov, and C. Ryan (2003a), The evolution of lithospheric mantle beneath the Kalahari Craton and its margins, *Lithos*, *71*, 215–241, doi:10.1016/j.lithos.2003.07.006.

Griffin, W. L., S. Y. O'Reilly, N. Abe, S. Aulbach, R. M. Davies, N. J. Pearson, B. J. Doyle, and K. Kivi (2003b), The origin and evolution of Archean lithospheric mantle, *Precambrian Res.*, *127*(1–3), 19–41, doi:10.1016/S0301-9268(03)00180-3.

Guillou-Frottier, L., E. Burov, S. Cloetingh, E. Le Goff, Y. Deschamps, B. Huet, and V. Bouchot (2012), Plume-induced dynamic instabilities near cratonic blocks: Implications for P-T-t paths and metallogeny, *Global Planet. Change*, *90–91*, 37–50, doi:10.1016/j.gloplacha.2011.10.007.

Hanghøj, K., and P. Kelemen (2001), Osmium isotopes in the Wiedemann Fjord mantle xenoliths: A unique record of cratonic mantle formation by melt depletion in the Archaean, *Geochem. Geophys. Geosyst.*, *2*(1), 1011, doi:10.1029/2000GC000085.

He, L. (2014), Numerical modeling of convective erosion and peridotite-melt interaction in big mantle wedge: Implications for the destruction of the North China Craton, *J. Geophys. Res. Solid Earth*, *119*(4), 3662–3677, doi:10.1002/2013JB010657.

Hill, R. I. (1991), Starting plumes and continental break-up, *Earth Planet. Sci. Lett.*, *104*(2–4), 398–416, doi:10.1016/0012-821X(91)90218-7.

Hirth, G., and D. L. Kohlstedt (1996), Water in the oceanic upper mantle: Implications for rheology, melt extraction and the evolution of the lithosphere, *Earth Planet. Sci. Lett.*, *144*(1–2), 93–108.

Holtzman, B. K., D. S. H. King, and D. L. Kohlstedt (2012), Effects of stress-driven melt segregation on the viscosity of rocks, *Earth Planet. Sci. Lett.*, *359–360*, 184–193, doi:10.1016/j.epsl.2012.09.030.

Houseman, G. A., and P. Molnar (1997), Gravitational (Rayleigh-Taylor) instability of a layer with non-linear viscosity and convective thinning of continental lithosphere, *Geophys. J. Int.*, *128*(1), 125–150, doi:10.1111/j.1365-246X.1997.tb04075.x.

Jackson, J. A., H. Austrheim, D. McKenzie, and K. Priestley (2004), Metastability, mechanical strength, and the support of mountain belts, *Geology*, *32*(7), 625–628, doi:10.1130/G20397.1.

James, D. E., M. J. Fouch, J. C. Vandecar, and S. Van Der Lee (2001), Tectospheric structure beneath southern Africa, *Geophys. Res. Lett.*, *28*(13), 2485–2488.

Janney, P. E., S. B. Shirey, R. W. Carlson, D. G. Pearson, D. R. Bell, A. P. Le Roex, A. Ishikawa, P. H. Nixon, and F. R. Boyd (2010), Age, composition and thermal characteristics of South African off-craton mantle lithosphere: Evidence for a multi-stage history, *J. Petrol.*, *51*(9), 1849–1890, doi:10.1093/petrology/egq041.

Jaupart, C., P. Molnar, and E. Cottrell (2007), Instability of a chemically dense layer heated from below and overlain by a deep less viscous fluid, *J. Fluid Mech.*, *572*, 433–469, doi:10.1017/S0022112006003521.

Karato, S. (2010), Rheology of the deep upper mantle and its implications for the preservation of the continental roots: A review, *Tectonophysics*, *481*(1–4), 82–98, doi:10.1016/j.tecto.2009.04.011.

King, S. D., C. Lee, P. E. Van Keken, W. Leng, S. Zhong, E. Tan, N. Tosi, and M. C. Kameyama (2010), A community benchmark for 2-D Cartesian compressible convection in the Earth's mantle, *Geophys. J. Int.*, *180*, 73–87, doi:10.1111/j.1365-246X.2009.04413.x.

Kobussen, A. F., W. L. Griffin, S. Y. O'Reilly, and S. R. Shee (2008), Ghosts of lithospheres past: Imaging an evolving lithospheric mantle in southern Africa, *Geology*, *36*(7), 515–518, doi:10.1130/G24868A.1.

Konzett, J., R. A. Armstrong, R. J. Sweeney, and W. Compston (1998), The timing of MARID metasomatism in the Kaapvaal mantle: An ion probe study of zircons from MARID xenoliths, *Earth Planet. Sci. Lett.*, *160*, 133–145.

Krystopowicz, N. J., and C. A. Currie (2013), Crustal eclogitization and lithosphere delamination in orogens, *Earth Planet. Sci. Lett.*, *361*, 195–207, doi:10.1016/j.epsl.2012.09.056.

Lee, C.-T. A., P. Luffi, and E. J. Chin (2011), Building and destroying continental mantle, *Annu. Rev. Earth Planet. Sci.*, *39*(1), 59–90, doi:10.1146/annurev-earth-040610-133505.

Lenardic, A., and L. Moresi (1999), Some thoughts on the stability of cratonic lithosphere: Effects of buoyancy and viscosity, *J. Geophys. Res.*, *104*(B6), 12,747–12,758.

Levander, A., B. Schmandt, M. S. Miller, K. Liu, K. E. Karlstrom, R. S. Crow, C.-T. A. Lee, and E. D. Humphreys (2011), Continuing Colorado plateau uplift by delamination-style convective lithospheric downwelling, *Nature*, *472*(7344), 461–465, doi:10.1038/nature10001.

Li, Z.-X., and S. Zhong (2009), Supercontinent-superplume coupling, true polar wander and plume mobility: Plate dominance in whole-mantle tectonics, *Phys. Earth Planet. Inter.*, *176*(3–4), 143–156, doi:10.1016/j.pepi.2009.05.004.

Manglik, A., and U. R. Christensen (1997), Effect of mantle depletion buoyancy on plume flow and melting beneath a stationary plate, *J. Geophys. Res.*, *102*(B3), 5019–5028, doi:10.1029/96JB03623.

Mather, K. A., D. G. Pearson, D. McKenzie, B. A. Kjarsgaard, and K. Priestley (2011), Constraints on the depth and thermal history of cratonic lithosphere from peridotite xenoliths, xenocrysts and seismology, *Lithos*, *125*(1–2), 729–742, doi:10.1016/j.lithos.2011.04.003.

Menzies, M. A., W. Fan, and M. Zhang (1993), Palaeozoic and Cenozoic lithoprobes and the loss of >120 km of Archaean lithosphere, Sino-Korean craton, China, *Geol. Soc. Spec. Publ.*, *76*(1), 71–81, doi:10.1144/GSL.SP.1993.076.01.04.

Morency, C., M.-P. Doin, and C. Dumoulin (2002), Convective destabilization of a thickened continental lithosphere, *Earth Planet. Sci. Lett.*, *202*(2), 303–320, doi:10.1016/S0012-821X(02)00753-7.

Moresi, L.-N., and V. S. Solomatov (1995), Numerical investigation of 2D convection with extremely large viscosity variations, *Phys. Fluids*, *7*(9), 2154–2162, doi:10.1063/1.868465.

Niu, Y. (2005), Generation and Evolution of Basaltic Magmas: Some Basic Concepts and a New View on the Origin of Mesozoic-Cenozoic Basaltic Volcanism in Eastern China, *Geol. J. Chine Univ.*, *11*(1), 9–46.

Nyblade, A., and N. Sleep (2003), Long lasting epeirogenic uplift from mantle plumes and the origin of the Southern African Plateau, *Geochem. Geophys. Geosyst.*, *4*(12), 1105, doi:10.1029/2003GC000573.

O'Connor, J. M., W. Jokat, A. P. le Roex, C. Class, J. R. Wijbrans, S. Keßling, K. F. Kuiper, and O. Nebel (2012), Hotspot trails in the South Atlantic controlled by plume and plate tectonic processes, *Nat. Geosci.*, *5*(10), 735–738, doi:10.1038/ngeo1583.

O'Neill, C. J., A. Lenardic, W. L. Griffin, and S. Y. O'Reilly (2008), Dynamics of cratons in an evolving mantle, *Lithos*, *102*(1–2), 12–24, doi:10.1016/j.lithos.2007.04.006.

Pearson, D. G., and G. M. Nowell (2002), The continental lithospheric mantle: Characteristics and significance as a mantle reservoir, *Philos. Trans. R. Soc. London A*, *360*(1800), 2383–410, doi:10.1098/rsta.2002.1074.

Pearson, D. G., and N. Wittig (2008), Formation of Archaean continental lithosphere and its diamonds: The root of the problem, *J. Geol. Soc.*, *165*(5), 895–914, doi:10.1144/0016-76492008-003.

Pearson, D. G., and N. Wittig (2014), The formation and evolution of cratonic mantle lithosphere—Evidence from mantle xenoliths, in *The Mantle & Core, Treat. on Geochem.*, vol. 3, edited by R. W. Carlson and H. D. Holland, pp. 225–292, Elsevier, Oxford, U. K.

Pearson, D. G., G. J. Irvine, D. A. Ionov, F. R. Boyd, and G. E. Dreibus (2004), Re-Os isotope systematics and platinum group element fractionation during mantle melt extraction: A study of massif and xenolith peridotite suites, *Chem. Geol.*, *208*(1–4), 29–59, doi:10.1016/j.chemgeo.2004.04.005.

Pearson, D. G., et al. (2014), Hydrous mantle transition zone indicated by ringwoodite included within diamond, *Nature*, *507*, 221–224.

Peslier, A. H., A. B. Woodland, D. R. Bell, M. Lazarov, and T. J. Lapen (2012), Metasomatic control of water contents in the Kaapvaal cratonic mantle, *Geochim. Cosmochim. Acta*, *97*, 213–246, doi:10.1016/j.gca.2012.08.028.

Poudjom Djomani, Y. H., W. L. Griffin, S. Y. O'Reilly, and B. J. Doyle (2005), Lithospheric domains and controls on kimberlite emplacement, Slave Province, Canada: Evidence from elastic thickness and upper mantle composition, *Geochem. Geophys. Geosyst.*, *6*, Q10006, doi: 10.1029/2005GC000978.

Priestley, K., and D. McKenzie (2013), The relationship between shear wave velocity, temperature, attenuation and viscosity in the shallow part of the mantle, *Earth Planet. Sci. Lett.*, *381*, 78–91, doi:10.1016/j.epsl.2013.08.022.

Ribe, N. M., and U. R. Christensen (1994), Three-dimensional modeling of plume-lithosphere interaction, *J. Geophys. Res.*, *99*(B1), 669–682, doi:10.1029/93JB02386.

Richard, G. C., and H. Iwamori (2010), Stagnant slab, wet plumes and Cenozoic volcanism in East Asia, *Phys. Earth Planet. Inter.*, *183*(1–2), 280–287, doi:10.1016/j.pepi.2010.02.009.

Rudnick, R. L., W. F. McDonough, and R. J. O'Connell (1998), Thermal structure, thickness and composition of continental lithosphere, *Chem. Geol.*, *145*(3–4), 395–411, doi:10.1016/S0009-2541(97)00151-4.

Sand, K. K., T. E. Waight, D. G. Pearson, T. F. D. Nielsen, E. Makovicky, and M. T. Hutchison (2009), The lithospheric mantle below southern West Greenland: A geothermobarometric approach to diamond potential and mantle stratigraphy, *Lithos*, *112*, 1155–1166, doi:10.1016/j.lithos.2009.05.012.

Schmeling, H., and H. Wallner (2012), Magmatic lithospheric heating and weakening during continental rifting: A simple scaling law, a 2-D thermomechanical rifting model and the East African Rift System, *Geochem. Geophys. Geosyst.*, *13*, Q08001, doi:10.1029/2012GC004178.

Schmeling, H., et al. (2008), A benchmark comparison of spontaneous subduction models—Towards a free surface, *Phys. Earth Planet. Inter.*, *171*(1–4), 198–223, doi:10.1016/j.pepi.2008.06.028.

Schutt, D. L., and C. E. Lesher (2010), Compositional trends among Kaapvaal Craton garnet peridotite xenoliths and their effects on seismic velocity and density, *Earth Planet. Sci. Lett.*, *300*(3–4), 367–373, doi:10.1016/j.epsl.2010.10.018.

Simon, N., G. R. Irvine, and G. Davies (2003), The origin of garnet and clinopyroxene in "depleted" Kaapvaal peridotites, *Lithos*, *71*(2–4), 289–322, doi:10.1016/S0024-4937(03)00118-X.

Sleep, N. H. (2003), Geodynamic implications of xenolith geotherms, *Geochem. Geophys. Geosyst.*, *4*(9), 1079, doi:10.1029/2003GC000511.

Sleep, N. H., C. J. Ebinger, and J.-M. Kendall (2002), Deflection of mantle plume material by cratonic keels, *Geol. Soc. Spec. Publ.*, *199*(1), 135–150, doi:10.1144/GSL.SP.2002.199.01.08.

Smit, K. V., D. G. Pearson, T. Stachel, and M. Seller (2014), Peridotites from Attawapiskat, Canada: Mesoproterozoic reworking of palaeoarchaean lithospheric mantle beneath the northern superior superterrane, *J. Petrol.*, *55*(9), 1829–1863, doi:10.1093/petrology/egu043.

Smith, D., and F. R. Boyd (1992) Compositional zonation in garnets of peridotite xenoliths, *Contrib. Miner. Petrol.*, *112*, 134–147.

Tang, Y., H. Zhang, J. Ying, and B. Su (2013), Widespread refertilization of cratonic and circum-cratonic lithospheric mantle, *Earth Sci. Rev.*, *118*, 45–68, doi:10.1016/j.earscirev.2013.01.004.

Tappe, S., S. F. Foley, A. Stracke, R. L. Romer, B. A. Kjarsgaard, L. M. Heaman, and N. Joyce (2007), Craton reactivation on the Labrador Sea margins: 40Ar/39Ar age and Sr-Nd-Hf-Pb isotope constraints from alkaline and carbonatite intrusives, *Earth Planet. Sci. Lett.*, *256*(3–4), 433–454, doi:10.1016/j.epsl.2007.01.036.

Tappe, S., D. G. Pearson, G. Nowell, T. Nielsen, P. Milstead, and K. Muehlenbachs (2011), A fresh isotopic look at Greenland kimberlites: Cratonic mantle lithosphere imprint on deep source signal, *Earth Planet. Sci. Lett.*, *305*(1–2), 235–248, doi:10.1016/j.epsl.2011.03.005.

Van Hunen, J., and S. Zhong (2003), New insight in the Hawaiian plume swell dynamics from scaling laws, *Geophys. Res. Lett.*, *30*(15), 1785, doi:10.1029/2003GL017646.

Van Hunen, J., A. P. Van Den Berg, and N. J. Vlaar (2000), A thermo-mechanical model of horizontal subduction below an overriding plate, *Earth Planet. Sci. Lett.*, *182*, 157–169.

Van Hunen, J., S. Zhong, N. M. Shapiro, and M. H. Ritzwoller (2005), New evidence for dislocation creep from 3-D geodynamic modeling of the Pacific upper mantle structure, *Earth Planet. Sci. Lett.*, *238*, 146–155, doi:10.1016/j.epsl.2005.07.006.

Van Keken, P., and C. Gable (1995), The interaction of a plume with a rheological boundary: A comparison between two-and three-dimensional models, *J. Geophys. Res.*, *100*(B10), 20,291–20,302.

Van Keken, P. E., S. D. King, H. Schmeling, U. R. Christensen, D. Neumeister, and M.-P. Doin (1997), A comparison of methods for the modeling of thermochemical convection, *J. Geophys. Res.*, *102*(B10), 22,477–22,495, doi:10.1029/97JB01353.

Wang, H., J. van Hunen, D. G. Pearson, and M. B. Allen (2014), Craton stability and longevity: The roles of composition-dependent rheology and buoyancy, *Earth Planet. Sci. Lett.*, *391*, 224–233, doi:10.1016/j.epsl.2014.01.038.

Wang, Y., J. Huang, and S. Zhong (2015), Episodic and multi-staged gravitational instability of cratonic lithosphere and its implications for reactivation of the North China Craton, *Geochem. Geophys. Geosyst.*, doi:10.1002/2014GC005681, in press.

Yoshida, M. (2013), Mantle temperature under drifting deformable continents during the supercontinent cycle, *Geophys. Res. Lett.*, *40*, 681–686, doi:10.1002/grl.50151.

Yu, C.-Q., W.-P. Chen, J.-Y. Ning, K. Tao, T.-L. Tseng, X.-D. Fang, Y. J. Chen, and R. D. van der Hilst (2012), Thick crust beneath the Ordos plateau: Implications for instability of the North China craton, *Earth Planet. Sci. Lett.*, *357–358*, 366–375, doi:10.1016/j.epsl.2012.09.027.

Zhao, D., Y. Tian, J. Lei, L. Liu, and S. Zheng (2009), Seismic image and origin of the Changbai intraplate volcano in East Asia: Role of big mantle wedge above the stagnant Pacific slab, *Phys. Earth Planet. Inter.*, *173*(3–4), 197–206, doi:10.1016/j.pepi.2008.11.009.

Zhong, S., and A. B. Watts (2002), Constraints on the dynamics of mantle plumes from uplift of the Hawaiian Islands, *Earth Planet. Sci. Lett.*, *203*, 105–116.

Zhong, S., M. T. Zuber, L. Moresi, and M. Gurnis (2000), Role of temperature-dependent viscosity and surface plates in spherical shell models of mantle convection, *J. Geophys. Res.*, *105*(B5), 11,063–11,082, doi:10.1029/2000JB900003.

Zhu, R., and T. Zheng (2009), Destruction geodynamics of the North China craton and its Paleoproterozoic plate tectonics, *Chin. Sci. Bull.*, *54*(19), 3354–3366, doi:10.1007/s11434-009-0451-5.